THE EUROPEAN
PHYSICAL JOURNAL C

CLYC as a neutron detector in low background conditions

J. Plaza[1,a] , V. Bécares[1], D. Cano-Ott[1], C. Gómez[1], T. Martínez[1], E. Mendoza[1], A. Pérez de Rada[1], V. Pesudo[1], J. C. Sáez-Vergara[1], R. Santorelli[1], D. Villamarín[1], A. Ianni[2,3], C. Peña[2], J. Balibrea-Correa[4,5,6], A. Boeltzig[4,3,7], G. Imbriani[5]

[1] Centro de Investigaciones Energéticas Medioambientales y Tecnológicas, Avda Complutense 40, 28040 Madrid, Spain
[2] Laboratorio Subterráneo de Canfranc, Paseo de los Ayerbe s/n, Canfranc-Estación, 22880 Huesca, Spain
[3] INFN, Laboratori Nazionali del Gran Sasso, Via G. Acitelli 22, 67100 Assergi, Italy
[4] Universitá degli Studi di Napoli "Federico II", Naples, Italy
[5] INFN Sezione di Napoli, 80126 Naples, Italy
[6] Present address: Instituto de Física Corpuscular, CSIC-Universidad de Valencia, 46071 Valencia, Spain
[7] Present address: Helmholtz-Zentrum Dresden-Rossendorf, Bautzner Landstrasse 400, 01328 Dresden, Germany

Abstract We report on the thermal neutron flux measurements carried out at the Laboratorio Subterráneo de Canfranc (LSC) with two commercial $2'' \times 2''$ CLYC detectors. The measurements were performed as part of an experimental campaign at LSC with ^{3}He detectors, for establishing the sensitivity limits and use of CLYCs in low background conditions. A careful characterization of the intrinsic α and γ-ray background in the detectors was required and done with dedicated measurements. It was found that the α activities in the two CLYC crystals differ by a factor of three, and the use of Monte Carlo simulations and a Bayesian unfolding method allowed us to determine the specific α activities from the ^{238}U and ^{232}Th decay chains. The simulations and unfolding also revealed that the γ-ray background registered in the detectors is dominated by the intrinsic activity of the components of the detector such as the aluminum housing and photo-multiplier and that the activity within the crystal is low in comparison. The data from the neutron flux measurements with the two detectors were analyzed with different methodologies: one based on an innovative α/neutron pulse shape discrimination method and one based on the subtraction of the intrinsic α background that masks the neutron signals in the region of interest. The neutron sensitivity of the CLYCs was calculated by Monte Carlo simulations with MCNP6 and GEANT4. The resulting thermal neutron fluxes are in good agreement with complementary flux measurement performed with ^{3}He detectors, but close to the detection limit imposed by the intrinsic α activity.

1 Introduction

In recent years, Cs_2LiYCl_6:Ce (CLYC) crystals have received attention due to their combined γ-ray and neutron radiation detection properties [1–3]. CLYC has a good intrinsic efficiency for detecting γ-rays and a good time ($\sim$1 ns) and energy ($\sim$5% at 662 KeV) resolutions. The thermal neutron detection is provided through the ^{6}Li(n$_{th}$, α)^{3}H reaction. Fast neutrons can also be detected via the ^{35}Cl(n,p)^{35}S reaction [4,5]. The different decay times of the scintillation components due to charged particles or γ-rays allow performing a pulse shape discrimination analysis for separating neutrons from γ-rays [6].

The study of rare events, like those involved in dark matter searches, reactions of interest in astrophysics or neutrino physics, implies a very low detection rate of the interactions of interest. The neutron and γ-ray environmental background of the facility is one of the limiting factors for the detection capabilities, and thus the detection of rare events requires going to underground facilities. But, despite the background being much lower than in surface laboratories, there is still a number of interactions that should be monitored and taken into account.

The aim of this paper is to measure the thermal neutron background at the Laboratorio Subterráneo de Canfranc (LSC, 2450 m.w.e.) using two commercial $2'' \times 2''$ CLYC detectors, to assess the sensitivity limits of these detectors in a low background environment.

A first characterization of one of the detectors was previously carried out in Hall A of LSC [6]. The measurements resulted in an internal α activity of $\sim$30 mBq/kg, caused by

[a] e-mail: julio.plaza@ciemat.es (corresponding author)

the ^{238}U and ^{232}Th decay chains. Another important finding was that the deposited energy spectrum produced by thermal neutrons overlaps in the same energy region as the α spectrum, thus limiting the capability of detecting low neutron fluxes. For this reason, a thorough characterization of the α and γ-ray intrinsic activity of the detectors has been performed.

The final values of the neutron background obtained with the two CLYCs are compared with each other and with previous neutron flux values determined with ^{3}He counters [7,8].

2 Experimental setup

Two commercial $2'' \times 2''$ CLYC-50-PHI-50-P118 model detectors from Radiation Monitoring Devices Inc. (RMD) [9] were used in this work. The first detector (hereafter referred to as CLYC-1) was characterized previously in [6], and has a known internal α activity of $\sim$30 mBq/kg, originated by the ^{238}U and ^{232}Th decay chains.

The other CLYC detector (referred to as CLYC-2) was provided to LSC by RMD with the expectation of having a lower α activity background. Both detectors consist of a cylindrical 50 mm diameter x 50 mm long CLYC crystal, with 95% ^{6}Li enrichment, coupled to a Hamamatsu R6233-100 super bialkali photo-multiplier tube (PMT).

The detectors were connected to DAISY Digital Acquisition System [10] consisting of a 4-channel fast digitizer from SP Devices [11]. The raw signals from the detector were digitized at 1 GSample/s and 14 bit resolution in a triggerless mode. The duration of each sampled pulse was 35 μs.

The digitized signals were processed using an RC filter followed by a Constant Fraction Discriminator (CFD) algorithm. The zero-crossing of the CFD was used to detect the presence of a signal in the digitized buffer. Basic parameters such as baseline, amplitude, and charge integration in different time windows were obtained [12,13]. After such processing, a γ-ray energy resolution of 4.9% at 662 keV was achieved for CLYC-1 and 5.2% for CLYC-2.

To assess the detection limits of the detectors, a characterization of their intrinsic activity is needed. Hence, different configurations were used:

- Bare detectors, placed two meters above the ground level, for the measurement of the environmental thermal neutron background in Hall A.
- Both CLYC detectors (1 and 2) inside a lead shielding of 10 cm and 25 cm thickness respectively to measure their intrinsic γ spectrum. The lead used presents a specific activity lower than 27 mBq/kg for ^{210}Pb.
- CLYC-1 was also taken to Laboratorio Nazionale del Gran Sasso (LNGS) for further testing. The γ intrinsic
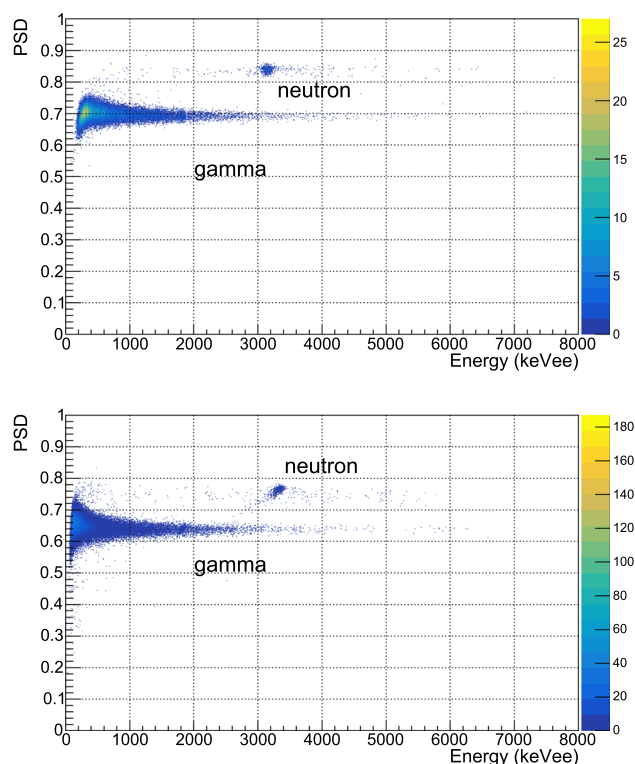

Fig. 1 Pulse shape discrimination with a moderated ^{252}Cf source. Top: CLYC-1. Bottom: CLYC-2

activity was also measured inside a 10 cm Pb Shielding with a N$_2$ flux.

- CLYC-2 inside a polyethylene shielding of 80x80x100 cm^3 (40 cm thickness of wall shielding) to obtain its intrinsic alpha spectrum, avoiding the neutron background contribution.

^{133}Ba, ^{137}Cs, and ^{88}Y sources were used for the calibration of the response to γ-rays, while a ^{252}Cf source inside a 1.4 cm thick polyethylene moderator was used for the calibration of the response to neutrons. The intrinsic α activity peaks were used for the energy calibration of the α spectra.

3 Pulse shape discrimination

One of the main attractive features of CLYC detectors is the excellent discrimination between γ-ray and neutron signals. A prompt and delayed area integration windows were defined to obtain a Pulse Shape Discrimination (PSD) parameter defined as:

$$PSD = \frac{A_{delayed}}{A_{prompt} + A_{delayed}} \tag{1}$$

The integration windows were optimized to achieve the best possible separation for each detector. Figure 1 shows the
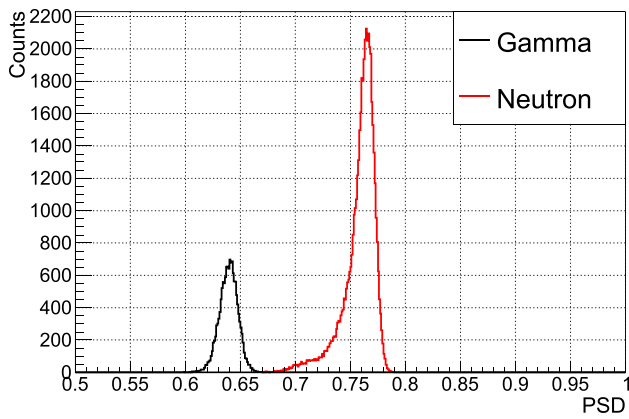
Fig. 2 PSD distribution for CLYC-2 in an energy range around the thermal neutron energy

PSD parameter versus total deposited energy for both detectors using the moderated ^{252}Cf calibration source. The spectra were calibrated in energy using the γ-ray sources. Neutron PSD values are higher than for γ-rays. The Regions Of Interest (ROIs) for thermal neutron detection appear around 3–3.5 MeVee. The selection of neutron events is made by choosing signals with a PSD > 0.79 for CLYC-1 and PSD > 0.7 for CLYC-2.

The figure of merit (FOM) quantifies how well the gamma region is separated from the neutron region. Its usual definition uses the centroid and FWHM of the PSD distribution in a certain energy range, assuming that the lobes for the two particle types follow a Gaussian distribution. However, from the discrimination plots for CLYC-2 in Fig. 1—Bottom and the PSD distribution in Fig. 2 it can be seen that the distribution is skewed and deviates from a Gaussian shape. Thus, we have redefined the FOM in a more general way as:

$$FOM = \frac{\mu_n - \mu_\gamma}{2.35 \cdot (\sigma_n + \sigma_\gamma)} \tag{2}$$

where μ and σ are the mean and standard deviation values of the PSD distributions for neutrons and γ-rays, while the 2.35 factor is used to make it equivalent to its original definition using the FWHM of a Gaussian distribution.

For CLYC-1, a FOM of 4.2 was obtained, in good agreement with its previous calculated value [6]. For CLYC-2 this value is reduced to 2.12.

In low background conditions, the count rate of the intrinsic α signals within the crystal is comparable to the thermal neutron count rate. Furthermore, the discrimination plot shows that these signals have similar PSD values, and also overlap with the deposited energy of neutrons (Fig. 3).

For each detector, average signals were obtained for α's, γ-rays and neutrons, for investigating a possible separation of the three types of particles. The neutron and γ-ray signals were obtained using the calibration runs, while α signals
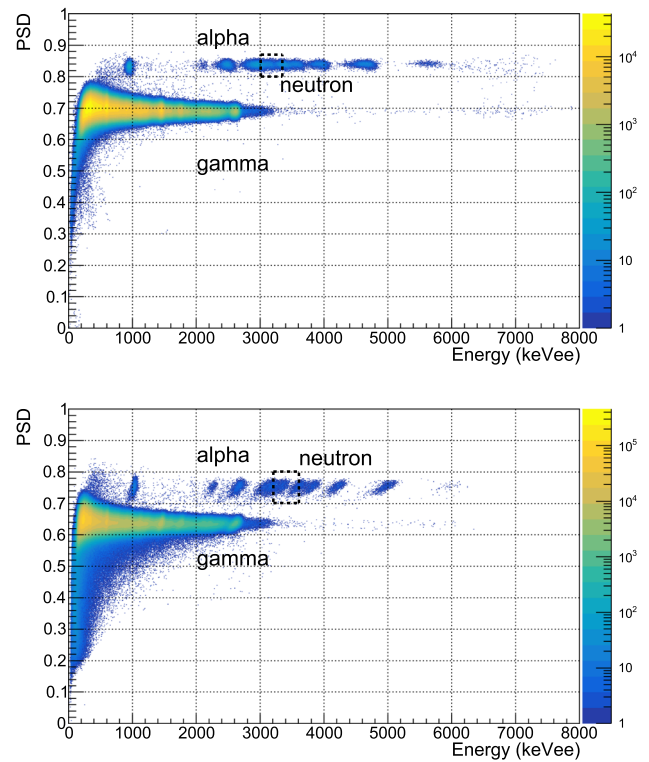

Fig. 3 Pulse shape discrimination of the background measurements. Top: CLYC-1. Bottom: CLYC-2. Dashed lines mark the region where neutron signals overlap with α signals

were taken from regions where neutrons are not present. The average signals for CLYC-1 and CLYC-2 are shown in Fig. 4.

The averaged signals were implemented on a True Shape Fit algorithm [14], where the digitized pulses were fitted to γ-ray, neutron, and α average shapes. The discrimination parameter to separate both signals uses the χ^2 values resulting from each fit and is defined as:

$$\frac{\Delta \chi^2}{A_{Fit}} = \frac{\chi_\gamma^2 - \chi_n^2}{A_{Fit}} \tag{3}$$

where A_{Fit} is the fitted amplitude. Figure 5 shows the discrimination for both detectors using this parameter.

One advantage of the True Shape Fit method is the possibility of resolving piled-up signals. In particular, this feature is very useful since the ^{232}Th chain contains a β^- decay of ^{212}Bi followed by an α-decay of ^{212}Po with a half-life of 300 ns. This decay time is shorter than the length of a single signal, and only a true shape fit is capable of reconstructing the pile-up and yielding accurate energy values for both signals (Fig. 6). However, due to the different signal widths for CLYC-1 and CLYC-2, the algorithm was more effective for the latter when analyzing close pile-ups.
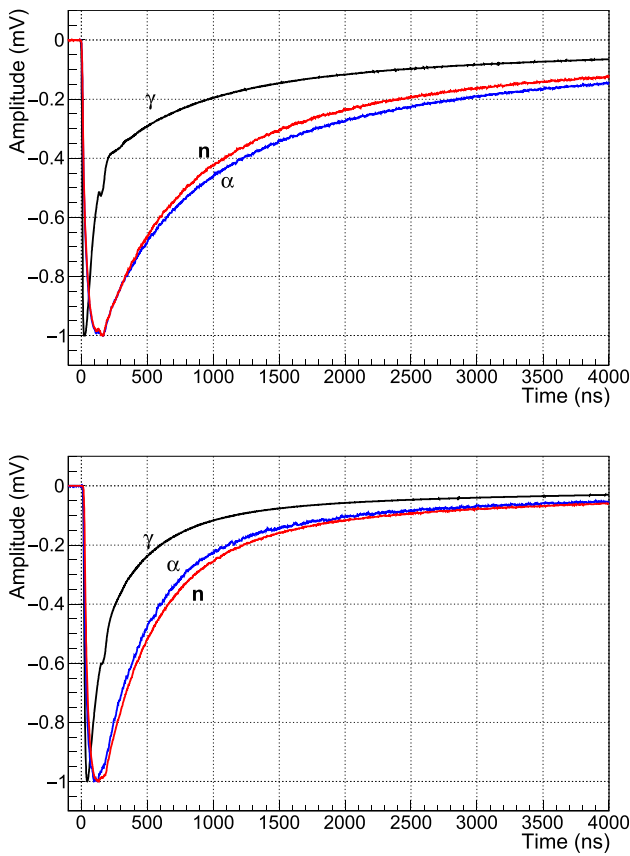
Fig. 4 Amplitude normalized average shapes for γ, neutron and α signals. Top: CLYC-1. Bottom: CLYC-2

Differences between CLYC-1 and CLYC-2 signals were investigated by fitting each signal to three decay components:

$$s(t) = \sum_i^3 \frac{f_i}{\tau_i} e^{-t/\tau_i} \tag{4}$$

where $s(t)$ is the signal shape, and f_i and τ_i are the fractions and decay times for each component. Table 1 lists the decay times and fractions for each component. For CLYC-1, these values are in consonance with values reported for other CLYC detectors [15].

In general, decay times of the slow components are shorter for CLYC-2. Also, the ratio of the fractions of fast to slow components is greater for CLYC-2. This suppression of the slower component correlates with the observed worse energy resolution of CLYC-2 relative to CLYC-1.

Pulse shape discrimination is possible due to the differences in the decay time of the fast components of each kind of signal. In that regard, the ratio of decay times of the fast components between neutron and γ signals is greater for CLYC-1, which relates to its better FOM.
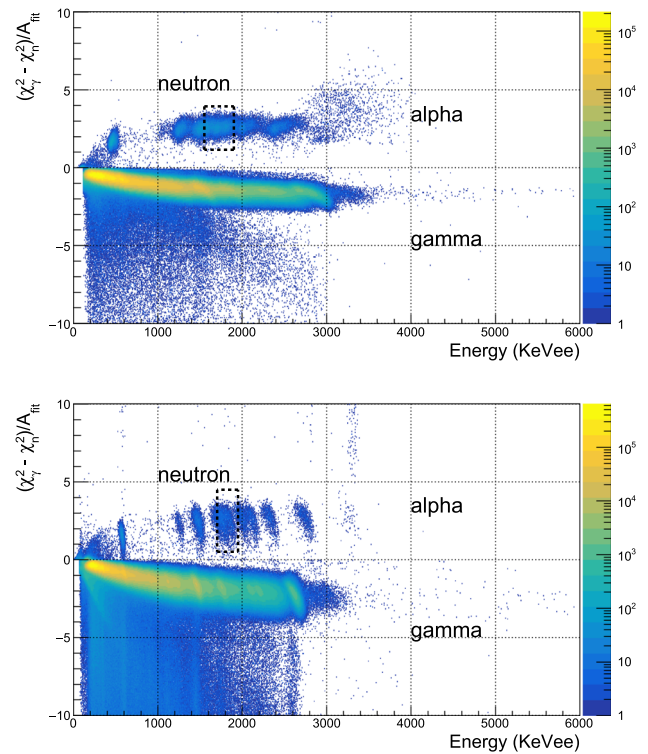

Fig. 5 Signal discrimination plots using the χ^2 value of the fit to an average γ and neutron shapes. Dashed lines represent the region where neutrons overlap with α's. Top: CLYC-1. Bottom: CLYC-2
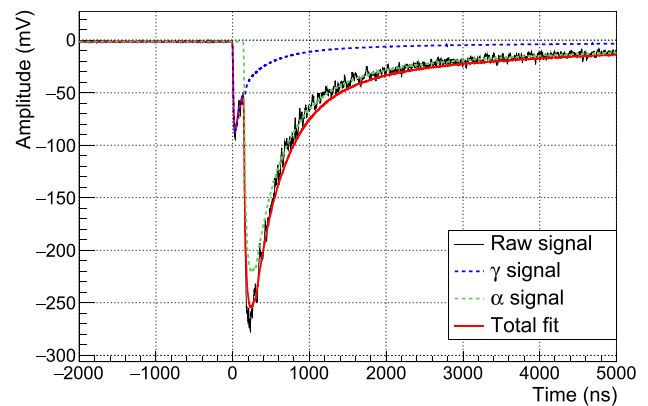

Fig. 6 Piled up signals with a time difference of 150 ns and reconstruction using a True Shape Fit

Lastly, for both detectors α signals behave in a very similar way to neutron signals. The small differences in the average signals fade away when real, noisy signals are considered. As a result, both signals overlap in the discrimination plots as observed.

CLYC-1 seems to qualitatively show a better chance to differentiate α from neutrons, and this is described in Sect. 6.

Table 1 Decay components and fractions for γ, neutron, and α signals. Uncertainties are of statistical nature only

	Fast	Intermediate	Slow
CLYC-1			
γ Decay time (ns)	66.6 ± 0.3	829 ± 2	5790 ± 2
Fractions (%)	5.26 ± 0.05	26.03 ± 0.10	68.71 ± 0.04
Decay time (ns)	373 ± 2	963 ± 3	5405 ± 4
n_{th} fractions (%)	8.80 ± 0.09	25.80 ± 0.23	65.39 ± 0.13
α fractions (%)	6.17 ± 0.04	23.74 ± 0.09	70.09 ± 0.07
CLYC-2			
γ Decay time (ns)	114.0 ± 0.4	523 ± 2	4559 ± 8
Fractions (%)	13.67 ± 0.06	33.4 ± 0.2	52.9 ± 0.2
Decay time (ns)	320 ± 1	787 ± 2	4565 ± 2
n_{th} fractions (%)	27.32 ± 0.07	22.47 ± 0.15	53.72 ± 0.06
α fractions (%)	28.95 ± 0.05	21.10 ± 0.07	49.95 ± 0.05

Table 2 Measured α activity in both detectors

	U/Th (mBq/kg)	Single peak (mBq/kg)	Total (mBq/kg)
CLYC-1	28.1 ± 0.2	7.31 ± 0.07	35.4 ± 0.2
CLYC-2	8.55 ± 0.06	2.64 ± 0.03	11.19 ± 0.07

4 Alpha intrinsic activity

Alpha spectra for both detectors are shown in Fig. 7. CLYC-1 α signals were selected from the PSD plot to obtain the α spectrum. For CLYC-2, they were selected from the χ^2 discrimination plot. The spectra were calibrated in energy using the most identifiable α peaks in the U/Th region (decays of ^{238}U, ^{234}U, ^{216}Po, ^{214}Po, ^{212}Po). CLYC-1 spectrum taken at LNGS showed similar features for the α region.

The observed peaks can be separated into two types of α events: the structures observed from 4 to 9 MeV are α decays produced by the U/Th decay chains. The second feature is an apparently single peak around 2.3 MeV. This energy value, however, may be inaccurate as it is estimated from the calibration extrapolated to lower energies. Similar spectrum features showing a complex structure at high energies and a single peak at lower energy have also been reported in other elpasolite detectors [16,17]. Without a mass spectrometry analysis, our educated guess is that the peak corresponds to an α-emitter contamination of the CLYC crystal.

The activity for each feature in both detectors is shown in Table 2. The total activity for CLYC-2 is about three times lower than for CLYC-1. This difference might be caused by differences during the crystal growth or purification process of the raw materials. The reduction in activity is consistent in both ranges of energy, supporting the idea that the single peak is produced by an α particle emitted by the intrinsic activity of the crystal [6].
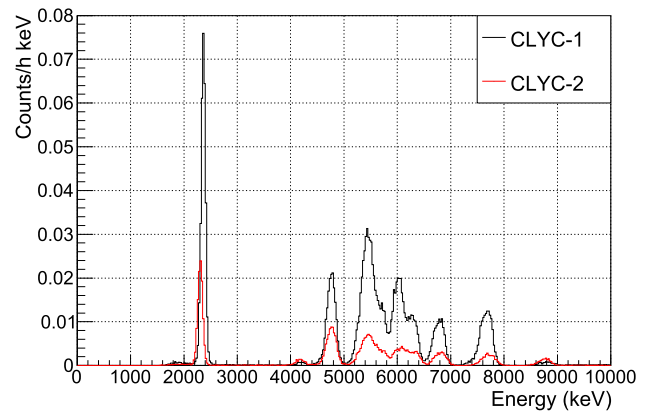

Fig. 7 Measured α spectra for CLYC-1 and CLYC-2

The Geant4 [18] Monte Carlo code was used to simulate the response of CLYC detectors to α particles. The geometry and material composition was modeled to the best of our knowledge. The responses to the ^{238}U and ^{232}Th decay chains were simulated assuming a uniform distribution of the isotopes inside the CLYC crystal. For each simulated event, the deposited energy from α particles was scored, and the results were used as the response functions to perform an unfolding of the experimental α spectra.

A resolution function of the form

$$\Delta E/E(\%) = \sqrt{a + b/E} \qquad (5)$$

was used to match the experimental resolution of the detectors, with $a = 1.31$, $b = 65698$ keV for CLYC-1, and $a = 0.181$, $b = 105007$ keV for CLYC-2.

A Bayesian method [19] was used for the unfolding (Fig. 8) of the α spectra. Isotopes from ^{238}U and ^{232}Th chains were identified, as well as a small contribution from ^{215}Po from the ^{235}U chain for CLYC-1, which was not present in CLYC-2. Table 3 lists all the isotopes and their specific activity for both detectors.

During the unfolding process, all activities varied freely without any constraint. Given the number of α emitters and overlaps in energy, isotopes were introduced into the unfolding as needed, starting with isolated peaks and with the most recognizable peaks.

The unfolded and experimental activities agree within the uncertainties. Unfolded CLYC-2 activites seem to be slightly higher than the experimental ones. The reconstruction of the spectrum involves different response functions that overlap, and tend to interfere and compensate between them. This leads to small features not always being correctly reproduced, as for instance an overestimation in the ^{220}Rn peak for CLYC-2 (Fig. 8 – bottom). Despite this fact, the results yield a situation close to secular equilibrium in both cases, which is to be expected.
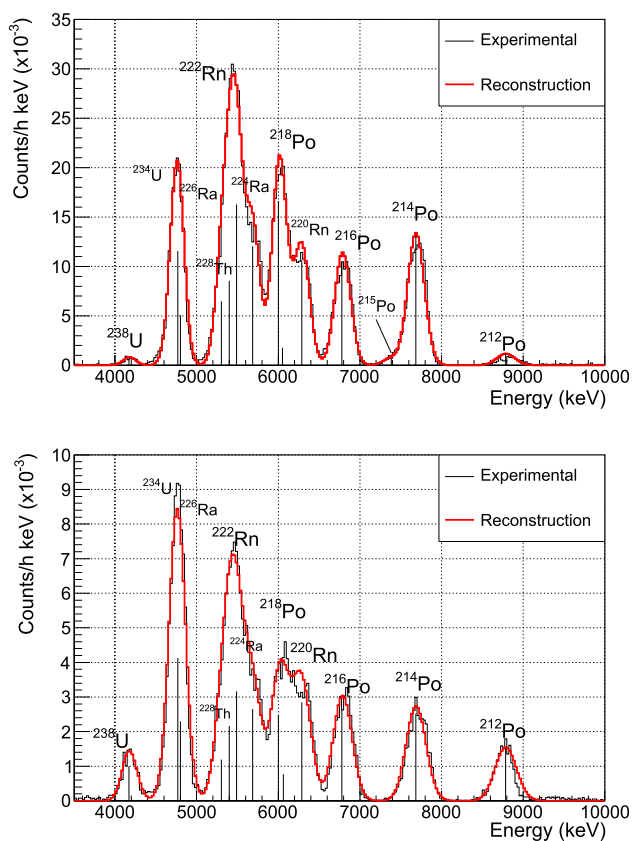
Fig. 8 Alpha spectrum and unfolding for CLYC-1 (Top) and CLYC-2 (Bottom). Only the main features are labeled

Table 3 Unfolded α activities. Uncertainties are only of statistical nature

Isotope	CLYC-1 (mBq/kg)	CLYC-2 (mBq/kg)
^{238}U	0.15 ± 0.01	0.31 ± 0.01
^{234}U	2.83 ± 0.13	1.27 ± 0.10
^{226}Ra	1.24 ± 0.13	0.71 ± 0.10
^{222}Rn	3.97 ± 0.13	0.97 ± 0.08
^{218}Po	4.06 ± 0.12	0.76 ± 0.07
^{214}Po	3.20 ± 0.05	0.78 ± 0.02
^{210}Po	1.58 ± 0.10	0.37 ± 0.06
^{228}Th	2.08 ± 0.19	0.67 ± 0.11
^{224}Ra	2.94 ± 0.06	0.82 ± 0.03
^{220}Rn	2.59 ± 0.05	0.88 ± 0.02
^{216}Po	2.54 ± 0.04	0.81 ± 0.02
^{212}Bi	0.44 ± 0.13	0.24 ± 0.07
^{212}Po	0.30 ± 0.01	0.47 ± 0.01
^{215}Po	0.24 ± 0.02	–
Unfolded activity	28.1 ± 0.4	8.7 ± 0.2

Alpha and neutron signals overlap in the 5.3 to 5.8 MeV range. That energy range is dominated by the ^{222}Rn and ^{224}Ra α-decays. For CLYC-1 they represent a count rate of 7.4

counts/h, while for CLYC-2 they correspond to 1.9 counts/h. These values impose a limit on the lowest directly detectable count rate of background neutrons if an α/neutron discrimination technique is not possible.

5 Gamma intrinsic activity

To obtain the intrinsic γ activity, both detectors were first placed inside 10 cm Pb shielding, and later the pulse discrimination cuts were applied to select the γ signals.

Geant4 simulations were also performed for simulating the response of the CLYCs to the U and Th decay chains in the crystal, with the isotopes and activities obtained from the analysis of the intrinsic α activity. The γ and β deposited energies were recorded to obtain the expected spectra. Figure 9 shows the measurements for the unshielded and shielded configurations (thick and thin solid lines) and the simulated spectra (dashed lines).

The measured spectra turned out to be one to two orders of magnitude larger than the results from the simulations. Considering that it may be due to the external background still being transmitted through the Pb shielding, CLYC-2 was again put inside a 25 cm thick shielding, to ensure that any external radiation was effectively blocked. However, the background level did not decrease.

Due to the differences in the shielding thicknesses, this shows that the external background was being effectively reduced in both cases. The source of the γ radiation has to be inside the shielding. This implies that the radiaton is related to the detectors themselves, but there are other contributions apart from the U and Th decay chains in the crystal. Different components of the detector such as the housings or photomultiplier may have a significant contribution to the intrinsic γ activity.

Another possible source is the inner wall of the shielding itself. The lead has a known specific activity less than 27 mBq/kg for ^{210}Pb, but there is no information about other isotopes.

The detectors show different responses. The main feature of CLYC-1 is a peak corresponding to the ^{40}K decay. ^{137}Cs can also be identified, whose origin might be in the CLYC crystal. γ spectra for CLYC-1 taken at LNGS showed a similar behaviour, with no difference between using a N_2 flux to purge possible Radon accumulation.

CLYC-2 shows lower activity in the ^{40}K peak and lower energy regions. In the higher energy region of the spectra, ^{208}Tl can be clearly identified for both detectors, with about the same activity.

With a fully assembled and operational detector, it is difficult to separate the origin and specific activity of each contaminant in the same way that a screening process on each individual component would do. Despite so, Geant4 simula-
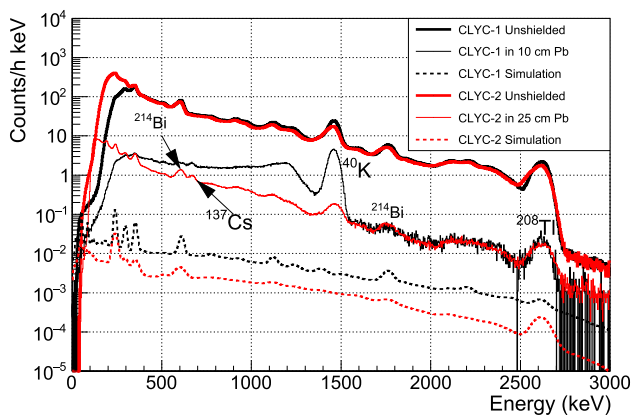
Fig. 9 Gamma spectrum for unshielded and shielded measurements. CLYC-1 was in a 10 cm Pb shield. CLYC-2 was in a 25 cm Pb shield. Dashed lines show the simulated intrinsic γ spectra in the CLYC crystals according to their unfolded α activities

tions were tentatively conducted to obtain response functions from different parts of the detector: ^{40}K was simulated in the aluminum housings, CLYC crystal and photo-multiplier; ^{137}Cs was simulated as a contaminant of the CLYC crystal; and ^{238}U and ^{232}Th chains were also simulated in the aluminum housings.

The same resolution function (Eq. 5) was used, with $a = 8.18$, $b = 7953$ keV for CLYC-1, and $a = 9.61$, $b = 12767$ keV for CLYC-2.

The same Bayesian unfolding was applied to the γ spectra, to separate the contribution and origin of each contaminant.

^{40}K originated at the aluminum housings turned out to be indistinguishable from that originated at the photo-multiplier. However, it is possible to obtain a different response for ^{40}K originated inside the CLYC crystal, due to the deposition of energy from β^- particles, and therefore, it is possible to separate both contributions. The Bayesian unfolding was able to reproduce the high energy region of the spectra, but for the lower energy region (<500 keV) we were not able to accurately reproduce it, meaning that there may be some contributions missing in the simulations. Table 4 summarizes the results obtained. The spectra, reconstruction, and the ^{40}K and ^{137}Cs unfolded contributions are shown in Fig. 10.

6 Thermal neutron background measurement

6.1 Neutron—alpha discrimination

As mentioned in Sect. 3, the signal shapes of CLYC-1 showed a small difference between α and neutron signals, hence offering the possibility of discriminating them. To this end, we have developed and applied a novel discrimination procedure.
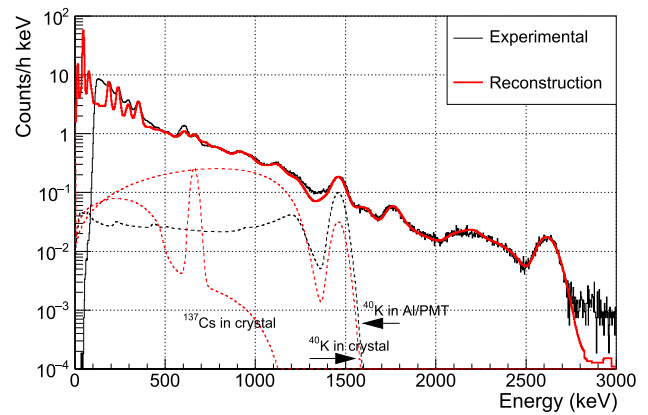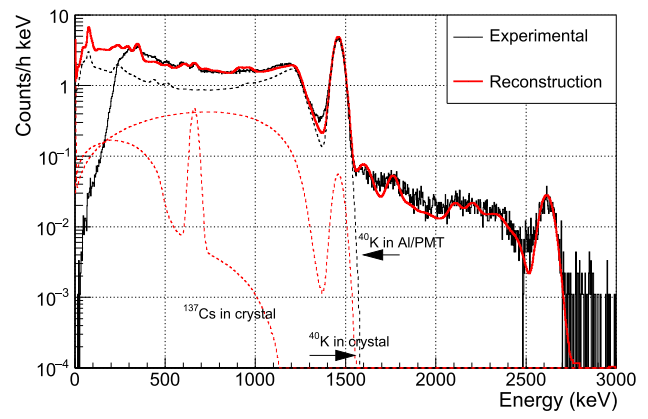

Fig. 10 Top: Experimental γ spectrum and unfolding for CLYC-1 in the 10 cm Pb shielding. Bottom: Experimental γ spectrum and unfolding for CLYC-2 in the 25 cm Pb shielding. Only ^{40}K and ^{137}Cs contributions have been plotted for clarity

Table 4 Gamma unfolded specific activities. ^{40}K origin cannot be uniquely attributed to the aluminum housing or the photo-multiplier

Isotope (source)	CLYC-1 (mBq/kg)	CLYC-2 (mBq/kg)
^{226}Ra (Housing)	–	13.37
^{228}Ac (Housing)	6.4	1.79
^{214}Bi (Housing)	0.69	0.65
^{208}Tl (Housing)	0.13	0.075
^{214}Pb (Housing)	22.4	33.35
^{212}Pb (Housing)	–	0.91
^{210}Pb (Housing)	–	73
^{212}Bi (Housing)	–	1.14
^{40}K (Housing/PMT)	372	1.8
^{40}K (CLYC crystal)	0.25	0.16
^{137}Cs (CLYC crystal)	0.05	0.03

The α and neutron signals were selected from the PSD discrimination plot. Each of the selected signals was fitted to the α and neutron average shapes and their respective χ^2_n and
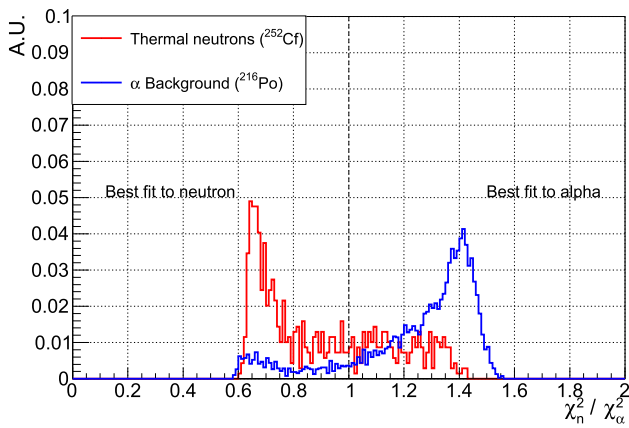
Fig. 11 Distributions of the relation of χ_n^2/χ_α^2 for neutron and α signals. Distributions are area-normalized for comparison purposes

χ_α^2 values were obtained. Figure 11 shows the distribution of the relation χ_n^2/χ_α^2 for two cases:

- Pure neutron signals, taken from the moderated ^{252}Cf calibration measurements and containing a negligible amount of α to the large neutron to α signal ratio.
- Pure α signals from the ^{216}Po decay taken from the background measurement and not overlapping with the neutron region of interest.

As can be seen, a fraction of neutron signals are best fitted to an α shape and analogously, a fraction of α signals are best fitted to a neutron shape. Since the resulting χ_n^2/χ_α^2 distributions are different for each case, we have developed an empirical method for quantifying the fraction of each signal type when both neutrons and α are mixed in a measurement.

From the pure neutron distribution, N_{Total} is the total number of neutrons. Let us define K_n as the fraction of them that are actually identified, or best–fitted, as neutrons (N_n):

$$N_n = K_n \cdot N_{Total} \tag{6}$$

Similarly, from the pure α distribution, the total number of α signals is A_{Total}, and we can define the fraction of them (K_α) which are best–fitted as neutrons (A_n):

$$A_n = K_\alpha \cdot A_{Total} \tag{7}$$

In a measurement where neutrons and α's mix and overlap, the region contains a total number of counts (M_{Total}) that is the sum of both neutrons and α's present in that region; then, let us define the fraction of mixed signals ($K_{\alpha n}$) that are best–fitted as neutrons (M_n)

$$M_n = K_{\alpha n} \cdot M_{Total} \tag{8}$$

In the extreme cases where there is a negligible amount of neutrons or α's, the value $K_{\alpha n}$ should tend to be either K_α or K_n, respectively. For the neutron background measurement at LSC, the count of both kinds of signals are not negligible and so the $K_{\alpha n}$ value will be something in between. A linear combination of K_n and K_α can be assumed to relate with $K_{\alpha n}$:

$$K_{\alpha n} = (1 - x)K_\alpha + x K_n \tag{9}$$

where x ranges from 0 to 1, and represents the fraction of neutrons present in the total counts. x can be easily obtained from Eq. (9):

$$x = \left(\frac{K_{\alpha n} - K_\alpha}{K_n - K_\alpha} \right) \tag{10}$$

And hence, the total number of neutrons can thus be calculated as:

$$N_{Total} = x M_{Total} \tag{11}$$

All the defined quantities K_n, K_α, $K_{\alpha n}$, and M_{Total} can be derived experimentally from the measurements performed:

- $K_n = 0.66 \pm 0.04$ is obtained from the moderated ^{252}Cf measurement.
- $K_\alpha = 0.147 \pm 0.007$ results from the background measurement, selecting a region free of neutrons, ^{216}Po in this case.
- $K_{\alpha n} = 0.208 \pm 0.008$ is obtained from the background measurement selecting the neutron region of interest.
- The total count of mixed neutron and alpha signals measured is $M_{Total} = 3479 \pm 59$

With these values, the fraction of actual neutrons in the region of interest is 12%, which yields a neutron count of 420 ± 80 neutrons in 1397 h of measurement, resulting in a count rate of 0.30 neutrons/h. As a reminder, the α count rate in the neutrons region of interest was 7.4 counts/h.

For CLYC-2, this pulse shape discrimination method was not possible due to the high similarity between α and neutron shapes, and the number of detected neutrons was obtained by subtracting the data measured inside the 40 cm polyethylene shielding (intrinsic detector background) from the unshielded data. Figure 12 shows the difference between the two spectra. The integration in the region of interest yielded a total of 409 $\pm$ 20 neutrons in 1397 h of measurement, resulting in a count rate of 0.29 neutrons/h, while the α count rate in that region was 1.4 counts/h.

The two neutron counting rates are compatible, as they should be since the two detectors are supposed to be identical and have the same ^{6}Li enrichment.
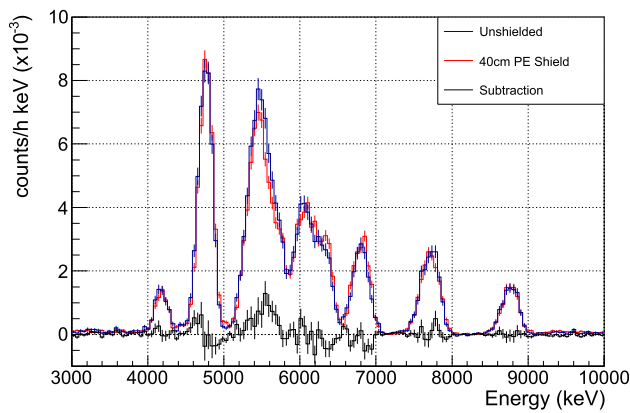
Fig. 12 CLYC-2 subtraction of PE shielding and unshielded runs to obtain the neutron count rate

6.2 Thermal neutron flux calculation

The general relationship between the count rate (R) of a detector and the flux Φ is expressed as:

$$R = \int \Phi(E) S(E) dE \qquad (12)$$

where S(E) is a sensitivity coefficient, dependent on the energy. In an experimental situation, the integral can be discretized to the sum of different energy intervals. In the case of a ^{6}Li enriched CLYC detector, mainly sensitive to thermal neutrons, we can use a unique energy interval centered around the thermal region, to obtain a flux value in that region. Equivalently, we can use a mean sensitivity coefficient of S for that region. In the case of an isotropic flux, the sensitivity is related to the detector intrinsic efficiency (ε) as [20,21]:

$$S = \frac{A\varepsilon}{4} \qquad (13)$$

where A is the total surface of the cylindrical CLYC crystal.

The Geant4 [18] and MCNP [22] Monte Carlo codes were used to obtain the efficiency and sensitivity to thermal neutrons. The response of the CLYC to an external isotropic neutron source, uniformly distributed over a sphere and following a Maxwellian distribution with T = 295 K was simulated. The intrinsic efficiency calculated with Geant4 amounts to 71.82 ± 0.02% (statistical) when only the ^{6}Li(n,α)^{3}H reactions are considered. The calculated sensitivity yielded a value of 20.06 ± 0.06 cm^2. MCNP simulations yielded an intrinsic efficiency of 73.19 ± 0.02% (statistical) and a sensitivity of 20.413 ± 0.005 cm^2. An average value of S = 20.23 cm^2 with a standard deviation of 0.18 cm^2 was adopted for calculating the neutron flux.

Using this value and the count rates from last section, the thermal flux results in $\Phi = (4.1 \pm 0.8) \times 10^{-6}$ n/cm^2 s for CLYC-1, and $\Phi = (4.0 \pm 0.2) \times 10^{-6}$ n/cm^2 s for CLYC-2.

The thermal neutron flux was also measured during the same period with two ^{3}He proportional detectors, and the calculated flux resulted in $\Phi = (3.9 \pm 0.2) \times 10^{-6}$ n/cm^{2}s as reported in [7]. The good agreement between the CLYC and ^{3}He is proof of the robustness of the different analysis methods and simulations involved and the correctness of the resulting thermal neutron flux value.

7 Conclusions

A thorough characterization of two CLYC detectors has been performed, with the purpose of establishing the sensitivity limits of these detectors in low background conditions.

Each detector produces different signals that affect the resolution and pulse shape discrimination capabilities. Specifically, CLYC-2 showed a suppressed slow component with respect to CLYC-1, which resulted in a degraded resolution and signal discrimination. The differences between the detectors may be caused by several factors, such as different activities of the raw materials, inhomogeneities of the crystal, the fraction of Ce doping, or other conditions during the crystal growth process.

The intrinsic α activity of the CLYC crystals was measured, obtaining a factor of three difference between them. An unfolding procedure was used to identify and quantify the α-emitters and their specific activities for each detector.

Based on these unfolded α activities, the expected γ activities from the U and Th chains were simulated and compared with measurements inside Pb shieldings. The results showed a much higher γ-ray background, indicating that there are far more significant contributions. Simulations suggest ^{137}Cs and ^{40}K may be present in the crystal, and that the aluminum housings, as well as the photo-multiplier, also represent important sources for the γ activity.

Despite the low CLYC intrinsic background, the neutron region of interest is masked by the overlapping α signals. This imposes a limit on the effectiveness of CLYCs as neutron detectors in low background conditions. Despite that, it was possible to measure the thermal neutron background at the Laboratorio Subterráneo de Canfranc thanks to a novel neutron/α discrimination procedure applied to CLYC-1 and a background subtraction applied to CLYC-2. The values obtained with the two CLYCs are in agreement and reproduce the previous result obtained with ^{3}He counters, thus assessing the robustness of the analysis methods applied and the correctness of the thermal neutron flux calculated.

Since the two CLYCs used in this work were not specifically built for underground measurements, their characteristics may potentially be improve, by using more radiopure materials for the crystals, detector housing, reflector, optical windows and photomultipliers.

Data availability statement   This manuscript has no associated data or the data will not be deposited. [Authors' comment: Data consists in several Gigabytes of data. They are kept at CIEMAT, and available upon request.].

References

1. J. Glodo et al., IEEE Trans. Nucl. Sci. **56**, 1257 (2009)
2. B. Budden et al., Nucl. Instr. Meth. A **784**, 97 (2015)
3. B.S. McDonald et al., Nucl. Instr. Meth. A **821**, 73 (2016)
4. N. D'Olympia et al., Nucl. Instr. Meth. A **694**, 140 (2012)
5. M.B. Smith et al., IEEE Trans. Nucl. Sci. **60**, 855 (2013)
6. T. Martínez et al., Nucl. Instr. Meth. A **906**, 150 (2018)
7. J. Plaza *et al.* Astropart. Phys. (2022), 102793. https://doi.org/10.1016/j.astropartphys.2022.102793
8. S.E.A. Orrigo, J.L. Tain, N. Mont-Geli et al., Eur. Phys. J. C **82**, 214 (2022). https://doi.org/10.1140/epjc/s10052-022-10755-6
9. RMD Inc. https://www.dynasil.com/company/radiation-monitoring-devices/
10. D. Villamarín et al. Nucl. Instr. Meth. A **1055**, 168526 (2023). https://doi.org/10.1016/j.nima.2023.168526
11. Teledyne SP Devices, https://www.spdevices.com
12. S. W. Smith, The Scientist and Engineer's Guide to Digital Signal Processing. California Technical Pub (1998). https://www.dspguide.com/
13. G.F. Knoll, Radiation detection and measurement, 4th ed. John Wiley & sons (2010)
14. C. Guerrero et al., Nucl. Instr. Meth. A **597**, 212 (2008)
15. X. Wen, A. Enqvist, Nucl. Instr. Meth. A **853**, 9 (2017)
16. R.S. Woolf et al., Nucl. Instr. Meth. A **838**, 147 (2016)
17. R.S. Woolf et al., Nucl. Instr. Meth. A **954**, 161228 (2020)
18. S. Agostinelli *et al.*, Nucl. Instr. Meth. A **506** (2003)
19. G. D'Agostini, Nucl. Instr. Meth. A **362**, 487 (1995)
20. A. K. Khokonov, Y. V. Savoiskii, A. V. Kamarazev, Phys. Atom. Nuclei, **73**(9), 1482 (2010)
21. J. Duderstadt, L. Hamilton. *Nuclear React. Anal.* John Wiley & Sons, New York (1976)
22. D. B. Pelowitz *et al.*, MCNP6 user's manual. Los Alamos National Laboratory report LA-CP-14-00745, (2014)